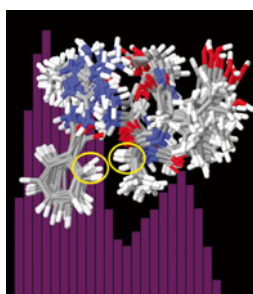


Exploring Radical Migration Pathways in Peptides with Positional Isomers, Deuterium Labeling, and Molecular Dynamics Simulations

Xing Zhang, Ryan R. Julian

Department of Chemistry, University of California, Riverside, CA 92521, USA



Abstract. One of the keys for understanding radical directed dissociation in peptides is a detailed knowledge of the factors that mediate radical migration. Peptide radicals can be created by a variety of means; however, in most circumstances, the originally created radicals must migrate to alternate locations in order to facilitate fragmentation such as backbone cleavage or side chain loss. The kinetics of radical migration are examined herein by comparing results from *ortho*-, *meta*-, and *para*-benzoyl radical positional isomers for several peptides. Isomers of a constrained cyclic peptide generated by several orthogonal radical initiators are also probed as a function of charge state. Cumulatively, the results suggest that small changes in radical position can significantly impact radical

migration, and overall structural flexibility of the peptide is also an important controlling factor. A particularly interesting pathway for the peptide RGYALG that is sensitive to *ortho* versus *meta* or *para* substitution was fully mapped out by a suite of deuterium labeled peptides. This data was then used to optimize parameters in molecular dynamics-based simulations, which were subsequently used to obtain further insight into the structural underpinnings that most strongly influence the kinetics of radical migration.

Key words: Kinetics, ECD, Photodissociation, Iodine

Received: 23 October 2012/Revised: 8 November 2012/Accepted: 9 November 2012/Published online: 30 January 2013

Introduction

Free radicals play various important roles in biology in both useful and destructive contexts [1]. For example, nitric oxide is a small endogenous diatomic radical that regulates blood flow. Radical chemistry is also key in the synthesis of nucleotides by ribonucleotide reductase for eventual synthesis of DNA. Reactive oxygen species such as hydroxyl and peroxide radicals are utilized beneficially by the immune system to attack invading organisms. On the other hand, reactive oxygen species are also byproducts of respiration or can be generated by other exogenous sources, and can harmfully attack lipids, proteins, and DNA [2].

Radical chemistry also plays an important role in mass spectrometry, where information about sequence and structure can be derived from the radical driven fragmentation of peptides or proteins via methods such as electron capture dissociation (ECD) or electron transfer dissociation (ETD). Both of these methods (at least initially) generate hydrogen-

abundant radicals, so called because the number of hydrogen atoms exceeds the number required for an even electron molecule. Most free radicals (including all discussed in the previous paragraph) are hydrogen deficient species, where essentially a hydrogen atom is missing relative to an even electron molecule. Collision induced dissociation (CID) based methods have been recently developed to generate hydrogen deficient radical peptides in the gas phase through various modification strategies, including oxidative dissociation of peptide-metal complexes [3] homolytic cleavage of labile bonds such as nitrate ester [4], peroxy carbamate [5], azo [6], nitroso [7], tempo [8], etc. One typical concern in generating radical peptides by CID is that charge directed backbone dissociation processes compete with desired radical generation, which may lead to suppression of radical yield in some situations. In comparison, photodissociation (PD) is capable of generating radical biomolecules via dissociative excited state chemistry that results in homolytic bond cleavage at specific chromophores. In particular, 266 nm UV photons can selectively cleave carbon–iodine (C–I), carbon–sulfur, or sulfur–sulfur bonds in modified peptides and proteins [9–11]. This method works independently of molecular size, and a single radical in a whole protein can easily be generated with

Electronic supplementary material The online version of this article (doi:10.1007/s13361-012-0540-6) contains supplementary material, which is available to authorized users.

Correspondence to: Ryan R. Julian; e-mail: ryan.julian@ucr.edu

high yield. The motivation for creating such radical species is that the fragmentation chemistry of hydrogen deficient radicals differs from that of even electron species, which enables unique experiments to be carried out. Radical directed dissociation of biomolecules in the gas phase can directly identify post-translational modification sites, distinguish peptide epimers, and even probe protein tertiary structure in vacuo [10, 12–14].

Radical directed dissociation (RDD) in hydrogen deficient radical peptides typically involves migration of the radical from the initial position where it was created to the site where dissociation is ultimately observed. These radical migration reactions, which all involve hydrogen atom transfers, are influenced by both thermodynamics and kinetics. The enthalpy of any given radical migration reaction can be easily estimated by determination of the relevant carbon–hydrogen (C–H) bond dissociation energies (BDEs) of both the radical donor and acceptor. Large BDEs indicate highly reactive radicals which will be enthalpically favored to migrate to sites with lower BDEs in the absence of kinetic constraints. Previously, we have shown that, on average, the relative abundance of backbone fragments and side chain losses observed for a series of peptides correlated well with the relevant BDEs; radical directed dissociation was favored for those sites with low C–H BDEs [15]. However, radical migration within any individual peptide will be kinetically influenced by the relevant activation energies, which are a function of three-dimensional structure and sequence-dependent steric constraints. For example, in very small, rigidly constrained peptides, high barriers to radical migration prevent radical isomerization and lead to different fragmentation patterns [16, 17]. On the other hand, similar fragmentation patterns have been observed in small flexible peptides, indicating that radical migration can also be facile [18, 19].

In the present work, we focus on kinetic constraints rather than thermodynamics. More specifically, we have examined a series of isomers where dissociation was investigated as a function of radical initiation site. For example, *ortho*-, *meta*-, and *para*- benzoyl radical modified peptide isomers reveal that even minor changes in radical initiation site can significantly influence subsequent dissociation pathways. A cyclic peptide yields virtually identical fragmentation patterns for three distinct radical isomers in the +1 charge state, yet the +2 charge state of the same peptide produces highly distinct dissociation spectra for all three isomers. In order to obtain more detailed structural insight into these results, we carried out molecular dynamics simulations. Deuterium labeling was used to experimentally map out one complete migration pathway, which was used to calibrate the molecular dynamics simulations. Subsequent investigation revealed that structural flexibility accounts for the different results in the +1 versus +2 charges states of the cyclic peptide. Alignment of the radical donors and acceptors is the primary controlling factor that distinguishes the results from *ortho* versus *meta* and *para* radical isomers.

Experimental

Materials

Peptides (RGYALG, RYLPT, cyclo-(RGDyK)) were purchased from American Peptide Company (Sunnyvale, CA, USA); 2-(hydroxymethyl-iodobenzoate)-18-crown-6 ether and *N*-hydroxysuccinimide (NHS) activated iodo-benzoyl ester were synthesized previously [20]. Sodium iodide, chloramine-T, sodium metabisulfite, and other organic solvents were purchased from Thermo-Fisher Scientific Pittsburgh, PA, USA. α -d₂-Glycine, α -d₁-alanine, iso-propyl-d₇-leucine and α -d₁-leucine were purchased from CDN Isotopes (Pointe-Claire, Quebec, Canada), while β -d₂-tyrosine was purchased from Cambridge Isotope Laboratories (Andover, MA, USA). Fmoc-protected amino acids were purchased from Anaspec (San Jose, CA, USA) or LC Sciences (Houston, TX, USA). Wang resin and 2,6-dichlorobenzoyl chloride (DCB) (Acros Organics, NJ, USA), fluorenylmethyloxycarbonyl-O-succinimide (Fmoc-oSu) and tetramethylammonium hexafluorophosphate (HCTU) (Chem-Pep Inc., Miami, FL, USA), isopropylsilane (TIPS) (Sigma-Aldrich, St. Louis, MO, USA) were also purchased.

Peptide Derivatization

Peptides were labeled at the *N*-terminus with NHS activated iodo-benzoyl ester (2× molar ratio) in 1:3 borate buffer (0.2 M, pH 8.5):dioxane solution for 30 min at 40 °C. The side product at arginine and tyrosine side chains were removed by incubation in 1 M hydroxylamine (adjusted pH to 8–9 by NaOH) for 4 h. Tyrosine in cyclo-(RGDyK) was iodinated with sodium iodide and chloramine-T at room temperature, after 1 min reaction time, excess sodium metabisulfite was added to quench the reaction. Stoichiometric quantities of reagents (1:2:1:2 molar ratio of peptide/sodium iodide/chloramine-T/sodium metabisulfite) were used to limit the iodination extent and produce mainly mono-iodinated tyrosine. A reversed phase cartridge (Michrom Bioresources, Inc., Auburn, CA, USA) was used for peptide desalting and purification.

Synthesis of Deuterium Labeled RGYALG

Fmoc protected amino acids (e.g., α -d₂-glycine, β -d₂-tyrosine, etc.) were synthesized by reaction with 1× Fmoc-oSu and 1× NaHCO₃ in 1:1 dioxane:H₂O solution overnight. After dissolving reaction mixture in 5 % HCl, the product was taken up using ethyl acetate and washed with 0.1 M HCl and water. Following drying with anhydrous Na₂SO₄, organic solvent was evaporated away and the protected amino acid was crystallized. Peptides were synthesized by solid phase methodology using Wang-resin and Fmoc chemistry. HCTU and piperidine was used for carboxyl group activation and amine group deprotection, respectively, whereas DCB was used for adding the first residue to Wang resin. Peptides were cleaved from the resin with 95:2.5:2.5 TFA:H₂O:TIPS.

Photodissociation Mass Spectrometry

Peptides (10 μM) were dissolved in 50:50 $\text{H}_2\text{O}:\text{CH}_3\text{OH}$ with 0.1 % acetic acid and electrosprayed into an LTQ linear quadrupole ion trap mass spectrometer (Thermo Fisher Scientific, San Jose, CA, USA). Fifty μM 2-(hydroxymethyl-iodobenzoate)-18-crown-6 ether was mixed with 10 μM peptide to form peptide-crown complexes; 266 nm photons were generated from the fourth harmonic generation of a Nd:YAG laser (Continuum, Santa Clara, CA, USA). The back plate of the instrument was modified with a quartz window to transmit UV photons into the linear ion trap. Laser pulses were synchronized to the isolation step via a digital delay generator. The isolation window for precursor ions in collision induced dissociation and photodissociation was set between 3 to 10 m/z with an activation value $q=0.25$ and default activation time 30 ms. For experiments utilizing deuterium labeled peptide to track the radical migration, the precursor ion isolation window was set at 1 m/z . Activation parameters were held constant for experiments where similarity scores are calculated.

Fragmentation Pattern Similarity Score

$$S = 1 - \frac{\sum_i |I_m^1(i) - I_m^2(i)|}{\sum_i I_m^1(i) + I_m^2(i)}$$

Of all ions (i), I_m^1 and I_m^2 are intensities of an ion at $m/z = "m"$ in two spectra excluding precursor ions [21]. A similarity score (S) value of 1 represents two spectra that are exactly the same. An in-house JAVA program was used to automatically calculate S from the peak lists of two mass spectra.

C–H Bond Dissociation Energy Calculations

GaussView 5.0 was used to build *N*-methyl-benzoylamide, which was used to model benzoic acid labeled peptides. Isodesmic reactions [22] were used to calculate C–H bond dissociation energies (BDEs) at *ortho*-, *meta*-, and *para*-positions of *N*-methyl-benzoylamide with $\text{C}_6\text{H}_5\text{-H}$ (472 kJ/mol) [23] as reference molecule. Energy calculations were performed at the B3LYP/6-31G(d) level of theory using Gaussian 09 ver. 8.0.

Molecular Modeling

MacroModel, ver. 9.9, (Schrödinger, LLC, New York, NY, USA) molecular mechanics software package was used to build benzoic acid modified RGYALG and cyclo-(RGDyK) and perform all molecular modeling simulations. Arginine side chains were protonated first, followed by lysine side chains for higher charge states. The OPLS force field [24]

was used for all calculations with the dielectric constant, $\epsilon=1.0$. Extended cutoffs were used for dipole–dipole interactions. Energy minimization was performed using the Polak-Ribiere conjugate gradient method with a derivative convergence criterion of 0.05 kJ/Å \cdot mol. Conformational searches with the Monte Carlo multiple minimum algorithm and enhanced torsional sampling were used with a maximum number of 10,000 steps; 100,000 conformations were saved with an interval of 0.1 ps during 10 ns molecular dynamics. We chose 500 K–750 K as molecular dynamics temperature to explore the peptide potential energy surface. These values are comparable to previous MD calculations for peptides in the gas phase and work well in our systems [25].

Results and Discussion

Fragmentation of *Ortho*-, *Meta*-, and *Para*-Iodobenzoyl Modified Peptide Radical Isomers

Radical isomers with the initial radical site at the *ortho*-, *meta*-, or *para*-position of the benzoyl group in *N*-iodobenzoyl-RGYALG were generated by 266 nm UV photodissociation to selectively cleave the photolabile C–I bonds and leave σ radicals on the benzene rings. The radical ions were subsequently re-isolated and subjected to CID as shown in Figure 1a–c. The results are typical for dissociation of a hydrogen deficient radical peptide [i.e., side chain losses (e.g., –43L, –56L, –106Y)] and selective backbone fragmentation (a_3 only) are observed [15]. Consecutive side chain losses are also observed in low abundance (e.g., –56L–CO $_2$, –43L–CO $_2$) suggesting multistep radical migrations occur to a lesser degree. Although the observed fragmentation channels for the *ortho*-, *meta*-, or *para*-benzoyl radical modified RGYALG isomers are very similar, there is some variation in the degree to which each dissociation channel is populated. In particular, the relative intensity for the a_3 ion from the *ortho*-radical isomer is significantly more abundant than is observed for the *meta*- and *para*-radical isomers. A similarity score (S , defined in experimental methods) is used to quantitatively characterize the similarity between two fragmentation patterns [21]. An S score of 1 implies that two spectra are identical with the same distributions of relative intensities; scores lower than 1 indicate less similarity. The reported similarity scores conservatively have uncertainties of ± 0.05 . Similarity scores are indicated with brackets between each pair of spectra in Figure 1. The *meta*-isomer (Figure 1b) is fairly similar ($S=0.85$) to the *para* isomer (Figure 1c), whereas the *ortho*-isomer is more distinct relative to both other spectra ($S=0.74, 0.59$ for *para* and *meta*, respectively). The lower scores for the *ortho*-isomer are primarily due to significantly increased peak intensity for the a_3 and leucine side chain loss fragments.

As an approximation to benzoic acid modified RGYALG, the BDEs for the *ortho*-, *meta*-, and *para*- C–H bonds in *N*-

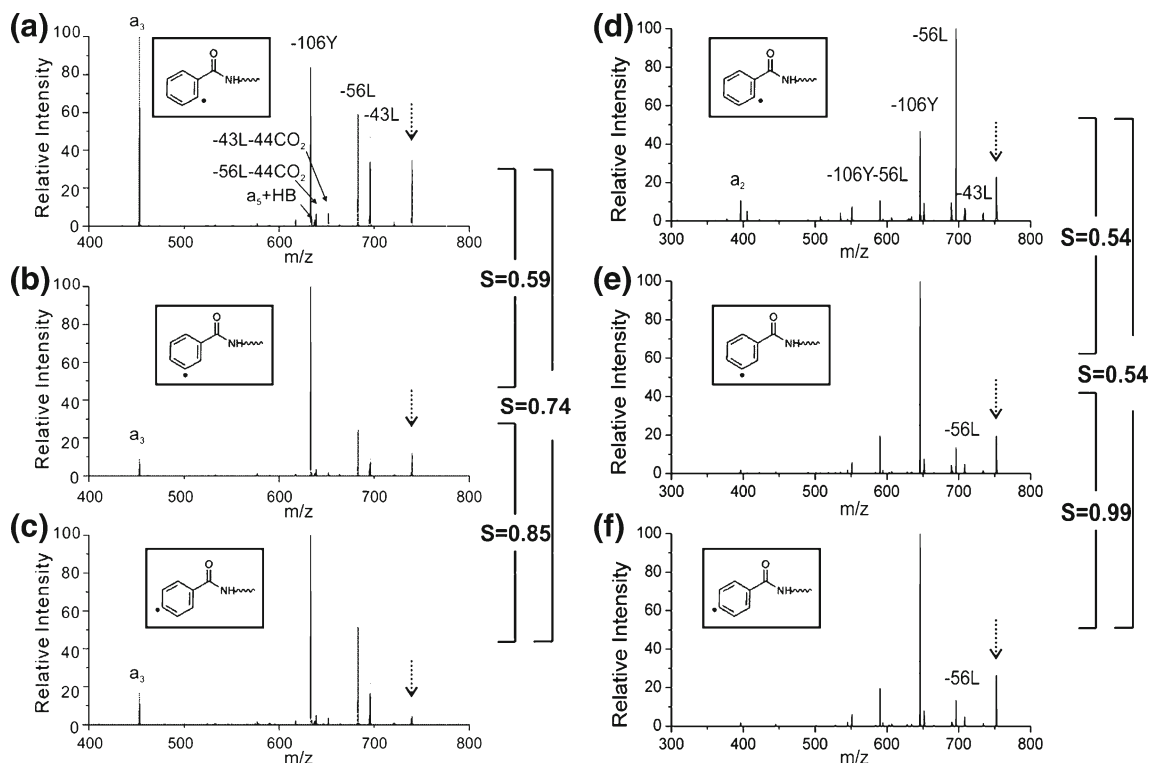


Figure 1. (a–c) CID spectrum of radical peptide *N*-benzoyl-RGYALG in the +1 charge state with initial radical at (a) *ortho*-, (b) *meta*-, or (c) *para*-position of benzoyl labeling group at *N*-terminus. (d–f) CID spectrum of radical peptide *N*-benzoyl-RYLPT in the +1 charge state with initial radical at (d) *ortho*-, (e) *meta*-, or (f) *para*-position of benzoyl labeling group at *N*-terminus. Side chain losses are abbreviated (i.e., –43L represents 43 Da side chain loss from leucine). Similarity scores (S) are indicated for each pair. The relevant radical precursor for each spectrum is indicated in the inset box, and precursor ions are indicated by a downward arrow

methyl-benzoylamide were calculated to be 461, 473, and 474 kJ/mol, respectively. These benzene radical isomers have very similar BDEs and are predicted to be very reactive (e.g., the C-H BDE values of all tertiary carbons in 20 amino acids range from 319 to 399 kJ/mol) [22]. Thermodynamics are therefore not anticipated to dictate the behavior of these radical isomers to any significant extent. The nature of our experiments, which utilize low energy collisional activation, should also favor kinetic products. The variations in fragmentation observed in Figure 1 are therefore most likely due to the influence of positional isomerism on relevant transition state geometries that dictate radical migration. The details of migration in this system were mapped out with deuterium labeling and molecular mechanics calculations that are reported further below.

Figure 1d–f show the CID spectra of radical isomers for another peptide, *N*-benzoyl-RYLPT. Side chain losses (e.g., –56L, –106Y) along with few radical initiated backbone fragmentations (e.g., a_2) are observed. The spectrum for the *meta*-isomer shown in Figure 1e is very similar to that for the *para*-isomer in Figure 1f ($S=0.99$). Thus for RYLPT, the *para* and *meta* positional isomers are essentially identical in terms of influence on radical migration kinetics. In contrast, the *ortho*-isomer yields an

obviously more distinct spectrum as shown in Figure 1d ($S=0.54, 0.54$). This is reminiscent of the results from the *N*-benzoyl-RGYALG isomers, where the *ortho*-isomer also exhibited the greatest difference. Taken together, these results suggest that the *ortho*-isomers are most distinct in terms of ability to influence the kinetics of radical migration. This observation is not unexpected given that both the *meta*- and *para*-isomers yield radicals, which are on the end of the benzoyl addition, whereas the *ortho*-isomer yields a radical that is directed back towards the point of attachment. Although it is clearly possible in some cases to accommodate the *para*-to-*meta*- shift by modest rotation or shifting of the benzoyl group, it is not possible to achieve similar alignment with the *ortho*-isomer.

Fragmentation of Cyclic Peptide Radical Isomers

A series of radical isomers for a small cyclic peptide cyclo-(RGDyK) (the small cap y indicates D-tyrosine) were subjected to collisional activation and the results are shown in Figure 2. These radical isomers were produced by several methods, and the radical initiator is identified within each spectrum. Figure 2a shows CID of the +1 cyclo-(RGDyK)[•]

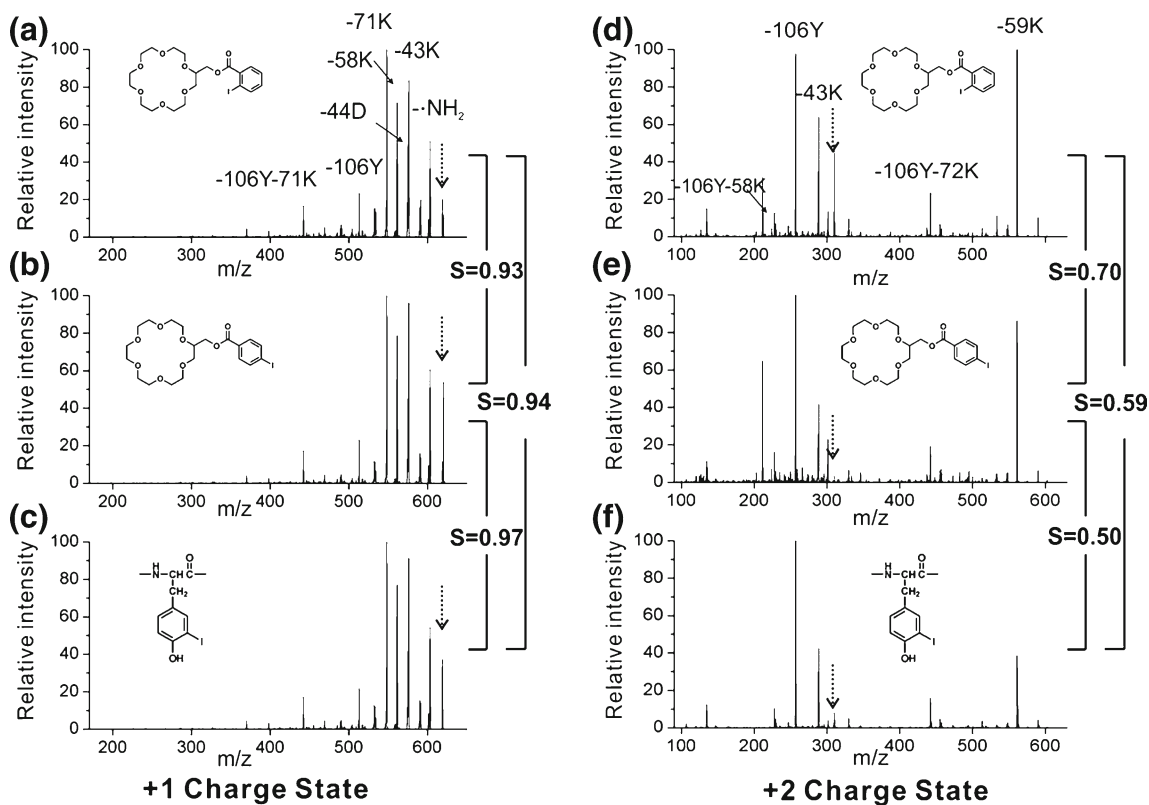
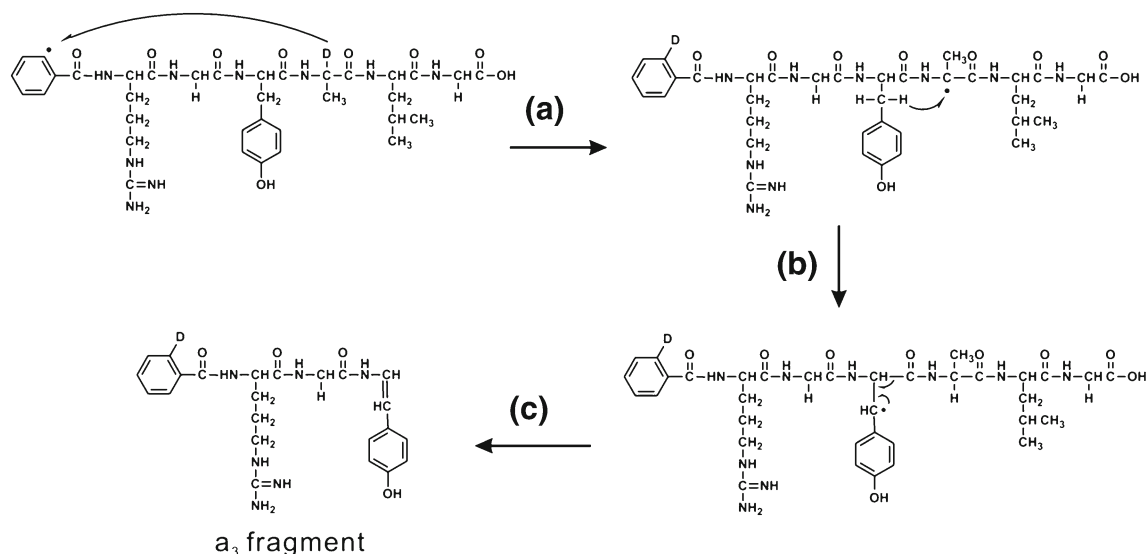


Figure 2. CID spectrum of cyclo-(RGDyK)⁺ in the +1 (a, b, c) and +2 (d, e, f) charge state with the radical introduced by *ortho*-iodobenzoyl modified 18-crown-6 based noncovalent radical delivery (a, d), *para*-iodobenzoyl modified 18-crown-6 (b, e) and tyrosine side chain iodination (c, f). Labeling of the spectra follows the same pattern established in Figure 1

radical isomer, which was produced by intermolecular radical migration [15]. In this method, a noncovalent complex between a peptide and a radical precursor (i.e., *ortho*-iodobenzoyl derivatized 18-crown-6) is isolated in the ion trap. The iodine atom in the radical precursor is then

selectively removed by photodissociation. The resulting phenyl radical is very reactive and abstracts a hydrogen atom from the peptide. Subsequent activation steps isolate and then fragment the peptide radical. In Figure 2b, a *para*-iodobenzoyl derivatized 18-crown-6 radical precursor was



Scheme 1. Radical migration pathway and β scission mechanism for generation of a_3 fragment from *N*-benzoyl-RGYALG with the initial radical at *ortho*-position of benzoyl group

used. In addition to the crown ether method, chemical iodination at tyrosine side chain was used as described previously [9]. Figure 2c shows the dissociation spectrum of cyclo-(RGDy•K) radical generated by tyrosine iodination. Most peaks in Figure 2a–c correspond to radical directed side chain losses from lysine ($-\text{NH}_2$, -43K , -58K , -71K), tyrosine (-106Y) and aspartic acid (-44D) residues. No backbone dissociation is detected, which is not surprising because at least two backbone bonds would need to be cleaved for fragmentation to be observable. A rich fragmentation pattern originating from the lysine side chain indicates that the radical can freely migrate to almost every carbon on its aliphatic chain [26]. Although the arginine side chain provides a similar target for radical attack, no side chain losses from arginine are observed. The arginine side chain is also the most probable location for protonation, which may enhance kinetic barriers via restricted conformational flexibility and could also complicate detection if the side chain loss retained the proton.

In Figure 2a and b, the initial sites where the radical transfers to the peptide are unknown. Given the steric differences caused by the *ortho* versus *para* substitution, it is unlikely that the initial sites are the same for Figure 2a and b. Similarly, it is unlikely that radical transfer via abstraction of an aromatic tyrosine hydrogen atom will occur due to enthalpic considerations [22]. Therefore, the precursor ions in Figure 2a, b, and c should all be different isomers of cyclo-(RGDyK)•. The striking similarity between all three spectra obtained by activation of the different isomers is therefore quite unexpected. Analogous experiments conducted on RGYALG yielded significantly less similar spectra (see supporting information).

The dissociation spectra for cyclo-(RGDyK)• isomers in Figure 2a–c have extremely high similarity scores (0.94, 0.97, and 0.93), indicating very little difference in fragmentation between the various isomers. This suggests that barriers to radical migration via numerous pathways for this peptide are likely low and comparable in magnitude. From an enthalpic standpoint, the radical sites which yield the fragments observed in Figure 2a–c are similar (BDEs ranging from 390 to 416 kJ/mol) [22]. A flat thermodynamic surface also favors a flat kinetic surface because endothermic reactions cannot contribute to kinetic barriers. Since the radicals initially start at different locations but ultimately yield very similar fragmentation patterns, the results further suggest that multiple migrations are occurring, which allows equilibration of the various isomers. The cyclic nature of the peptide restricts the overall available conformational space; however, this may actually facilitate interactions between the flexible lysine side chain and the remainder of the peptide, allowing migration to occur freely.

The situation changes dramatically when another charge is added to the peptide. Analogous experiments were conducted on the +2 charge state and are shown in Figure 2d, e, and f. The relative intensities of several side chain losses are notably different compared with those

observed in the +1 charge state. Interestingly, the similarity scores also change substantially (0.59, 0.50, 0.70), indicating that kinetic barriers are preventing the free migration observed in the +1 charge state. The addition of the second charge should occur on the side chain of lysine, which is by far the most basic available site. Intramolecular solvation of the additional charged site and Coulombic repulsion between the charges will likely lead to significant stiffening of the peptide structure and restriction of side chain flexibility, which will both serve to increase kinetic barriers to migration. This hypothesis is supported by molecular modeling which will be discussed further below.

Pinpointing Radical Migration with Deuterium Isotope Labeling

In Figure 1a–c, the a_3 fragment intensity serves as a diagnostic feature to distinguish between the *ortho* and *meta* or *para* positional isomers. An abundant a_3 ion is only formed for the *ortho*-isomer, suggesting favorable kinetics exist for this migration pathway. In order to explore the structural features that lead to these favorable kinetics in greater detail, it is necessary to determine the exact migration route. It has been well established previously that immediately prior to formation of the a_3 ion, the radical must migrate to the tyrosine β carbon as shown in Scheme 1c [15, 27]. However, the radical could arrive at the tyrosine β carbon via direct migration or through a multistep route. To determine the exact radical migration pathway, we prepared a series of deuterium isotope labeled peptides. Collisional activation of deuterium labeled tyrosine (Tyr β d2) yields an abundant $a_3(\text{d1})$ ion as shown in Figure 3a. Direct migration of the initial radical would lead to deuterium on the N-terminus and generation of an $a_3(\text{d2})$ ion. The results are not consistent with direct migration but rather indicate that deuterium has migrated to a site within the ALG residues. It should be mentioned that some amount of direct migration cannot be completely excluded because a small quantity of $a_3(\text{d2})$ is observed in Figure 3a, but direct migration is clearly not the primary pathway. The results suggest that initial radical at the N-terminus migrates to an intermediate site within ALG first, followed by subsequent migration to the tyrosine β carbon.

In an attempt to determine which intermediate site within the ALG residues the *ortho*-benzoyl radical migrates to, additional deuterium labeled peptides (i.e., Gly6 α d2, Leu α d1, Leu d7 isopropyl, Ala α d1) were synthesized and the results are shown in Figure 3b–e, respectively. None of the labeling sites at Gly6 or Leu are attacked by the benzoyl radical, otherwise an $a_3(\text{d1})$ ion would be observed as the major peak in the isotope distribution. However, the observation of $a_3(\text{d1})$ in Figure 3e suggests that the Ala α deuterium was abstracted directly as shown in Scheme 1a. Successive radical migration from the Ala α carbon to the Tyr β carbon is expected to be a facile process through a transition state with a six-membered ring. Our previous work

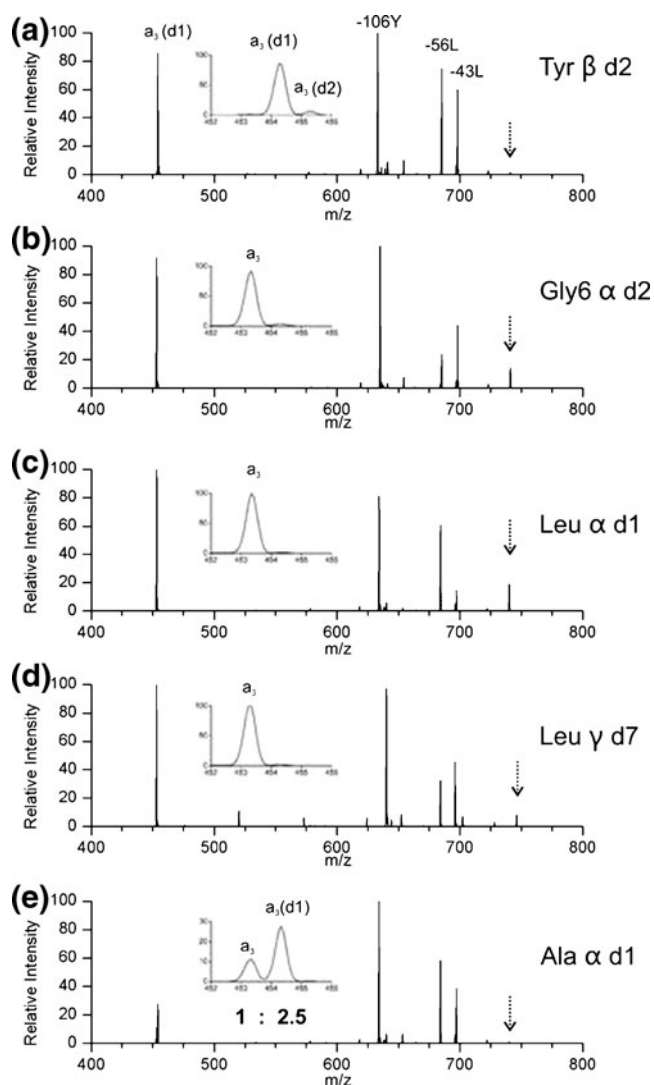


Figure 3. CID spectrum of *N*-benzoyl-RGYALG (+1) with radical at the *ortho*-position of benzoyl group and deuterium labeling at (a) Tyr β d2, (b) Gly6 α d2, (c) Leu α d1, (d) Leu γ d7 (isopropyl), and (e) Ala α d1. Down arrows indicate precursor ions

has shown that Tyr β radical can migrate from the carbon α position at an adjacent glycine residue [27]. Similarly, the Ala α radical should also be able to migrate to adjacent Tyr β carbon (Scheme 1b).

In order to determine if there are additional intermediate sites between the initial *ortho*-benzoyl radical and the Ala α carbon (Scheme 1a), the a₃(d1) isotope peak in Figure 3e was re-isolated and dissociated to identify the position of the deuterium. A benzoyl fragment containing a deuterium (Supplementary Figure S2) suggests that the Ala α deuterium was abstracted directly by the benzoyl radical. Data from deuterium labeling at the Gly2 α position also suggests that Gly2 α hydrogens are not involved in the major fragmentation pathway for a₃ ion (Supplementary Figure S3). It is worth noting that observation of the a₃(d0) isotope peak in

Figure 3e is inconsistent with the proposed two step migration mechanism (Scheme 1) suggesting the existence of other minor migration routes not involving the Ala α carbon. The intensity ratio between a₃(d0) and a₃(d1) is 1 : 2.5 in Figure 3e, suggesting the major pathway is the one outlined in Scheme 1. Kinetic isotope effects further support radical migration involving the Ala α hydrogen. The intensity of the a₃ ion in Figure 3e decreases significantly compared to that of the unlabeled peptide (see Figure 1a), which is consistent with a kinetic isotope effect disfavoring abstraction of deuterium.

Figure 4 shows the dissociation spectra of *meta*- and *para*-benzoyl radical RGYA(α d1)LG isomers. In contrast to *ortho*-isomer in Figure 3e, observation of a₃(d0) ion as the major isotope peak in Figure 4 indicates that the radical migration via the Ala α carbon is not a major pathway to generate the a₃ fragment for these two isomers. The relative intensity ratio between a₃(d0) and a₃(d1) is 1 : 0.63 for the *meta*-radical isomer (Figure 4a) and 1 : 0.47 for the *para*-isomer (Figure 4b). Compared with the 1 : 2.5 ratio for the *ortho*-isomer in Figure 3e, the extent of radical migration to Ala α occurs with the following preference: *ortho* > *meta* > *para*. This is consistent with the spectra in Figure 1a–c showing that *ortho*-radical isomer has the largest relative intensity of a₃. This order is found to be related to peptide 3D structure based on molecular dynamics calculations as discussed below.

Molecular Modeling

Conformational searches and molecular dynamics (MD) simulations were carried out to determine in greater detail

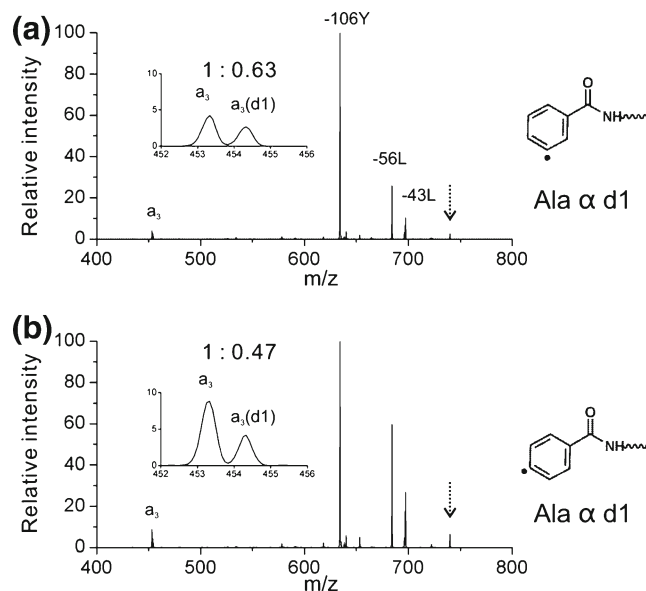


Figure 4. CID spectrum of *N*-benzoyl-RGYA(α d1)LG (+1) radical isomers with deuterium labeling at Ala α d1 and radical at the *meta*- position (a) and *para*- position (b) of the benzoyl group. Downward arrows indicate precursor ions

the influence of peptide structure and dynamics on radical migration. Force field parameters for odd-electron radicals are not readily available, so saturated peptides were constructed instead. Distances between hydrogen atoms representing potential radical donor and acceptor sites were monitored in lieu of calculating distances involving actual radical sites.

N-Benzoyl-RGYALG

The lowest potential energy structure for *N*-benzoyl-RGYALG obtained from a molecular mechanics conformational search is shown in Figure 5a. Interestingly, the *N*-terminal benzoyl group is very close to the alanine residue, which should kinetically facilitate radical migration from the benzoyl group to the Ala α carbon. In an attempt to understand why the *ortho*-benzoyl radical isomer favors radical migration to the Ala α carbon more than the other two isomers, the distances from the Ala α hydrogen to benzoyl *ortho*-, *meta*-, and *para*-hydrogens, were monitored during a 10 ns MD simulation at 500 K. Because hydrogen transfer can only occur when the donor is in very close proximity to the acceptor, the probability of residue contact at a distance below 4 Å was calculated for 100,000 sampled structures (Supplementary Figure S4). The *ortho*-benzoyl hydrogen has the highest probability for close contact with the Ala α hydrogen (26 %), whereas the probabilities for the *meta*- and *para*-hydrogens are 8.6 % and 3.6 %, respectively. This trend is consistent with the experimental data on the extent of radical migration to the Ala α carbon which follows the same order: *ortho* > *meta* > *para*.

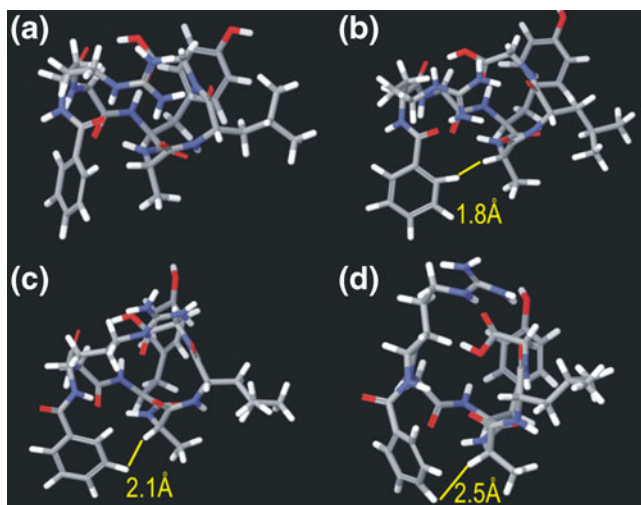


Figure 5. (a) The lowest potential energy structure of *N*-benzoyl-RGYALG resulting from a Monte Carlo multiple minimum conformational search; (b-d) structures with the smallest distance from the Ala α hydrogen to the *ortho*-benzoyl hydrogen, *meta*-benzoyl hydrogen, or *para*-benzoyl hydrogen obtained during 10 ns of MD simulations at 500 K are shown in (b), (c), (d), respectively

Figures 5b–d show the conformations obtained during molecular dynamics with the smallest distance from the Ala α hydrogen to the *ortho*- (Figure 5b), *meta*- (Figure 5c), or *para*- (Figure 5d) benzoyl hydrogen. All distances are smaller than 3 Å and should be satisfactory for radical migration; however, distance is not the only structural parameter that can influence radical migration kinetics. Hydrogen transfer preferentially proceeds via a linear or near-linear pathway in the transition state [28]. The alignment of bonds involved in potential hydrogen transfer from benzoyl *ortho*-hydrogen to the Ala α carbon (Figure 5b) is near-linear and thus optimal for hydrogen transfer. In comparison, the *meta*- and *para*-isomers have unfavorable nonlinear orientations and much higher activation barriers are expected as a consequence. The average results are also consistent with these snapshots, with a significantly higher fraction of the *ortho*-hydrogen isomer exhibiting near linear alignment (see Supplementary Figure S5).

Cyclo-(RGDyK) in the +1 and +2 Charge State

The fragmentation similarities for cyclo-(RGDyK) radical isomers in Figure 2 vary with charge state. As suggested above, this may be caused by restricted conformational space in the +2 charge state, which may inhibit radical migration. We carried out MD simulations for both charge states and monitored several distances between side chains. Figure 6 shows the statistical analysis of distances from 100,000 conformations sampled during 10 ns of MD at 750 K. Distances from the tyrosine *ortho*-hydrogen (the initial radical site in tyrosine-iodinated peptide) to the lysine δ -hydrogen are quite different between the +2 (Figure 6a) and +1 (Figure 6b) charge states. In the +1 charge state, the peptide exhibits a very broad distribution of distances, suggesting fairly unbiased occupation of the conformational space. For the +2 charge state, two distinct populations are clearly observed. It should be mentioned that a slightly greater number of structures with close contact is observed in the +2 charge state, although the corresponding lysine side chain losses are not more abundant for the +2 charge state (Figure 2c and f). This may indicate that direct migration is not the primary mechanism that generates these fragments. The primary purpose of the data in Figure 6a and b is to illustrate potential differences in conformational space, not to elucidate migration pathways (as is the case in Supplementary Figures S4 and S5).

In Figure 6c and d, the distances between the arginine δ hydrogen and the lysine δ hydrogen are shown. Both side chains are potential intermediate radical migration sites. In the +2 charge state, the protonation sites are most likely at lysine and arginine which leads to greater separation in space (>6 Å) as shown in Figure 6c. In comparison, there is some contact (distance below 4 Å) between lysine and arginine side chains in the +1 charge state (Figure 6d), which again suggests larger conformational space which should be

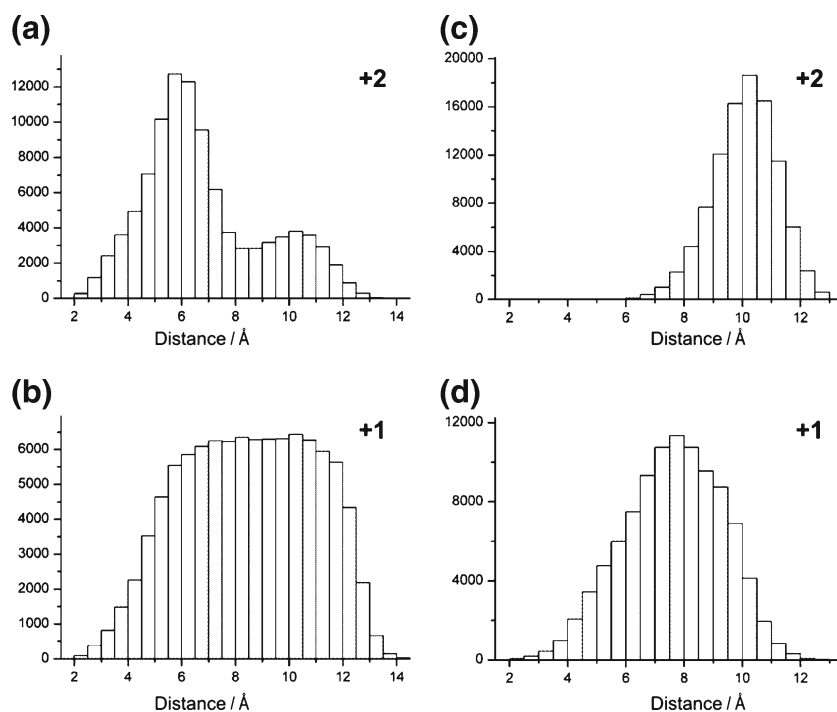


Figure 6. Histograms of monitored distances for cyclo-(RGDyK) in the +1 and +2 charge state during 10 ns molecular dynamics at 750 K from 100,000 sampled conformations. Distances between the *ortho*-hydrogen in tyrosine side chain and the δ -hydrogen in lysine are plotted in (a) for the +2 charge state and (b) for +1. Distances between the δ -hydrogen in arginine side chain and the δ -hydrogen in lysine side chain are plotted in (c) for the +2 charge state and (d) for +1

beneficial for radical migration. These MD simulations are consistent with the hypothesis that conformational flexibility and multiple migrations are the primary sources of the experimentally observed differences in dissociation between the +1 and +2 charge states as shown in Figure 2.

Conclusions

The present results illustrate that radical migrations in peptides are not unrestricted but can be significantly influenced by peptide 3D structure. Information on radical migration pathways can be derived from various approaches including evaluation of fragmentation pattern similarities among positional isomers, deuterium isotope labeling, and molecular mechanics calculations. For example, site specific deuterium labeling in RGYALG reveals that the initial *ortho*-benzoyl radical at *N*-terminus prefers migration to the tyrosine β carbon indirectly via the alanine α carbon as an intermediate site. However, this radical migration pathway is kinetically disfavored for *meta*- and *para*-radical isomers as a result of steric hindrance. The charge state dependent fragmentation pattern similarities among cyclo-(RGDyK)-isomers indicate that radical migration pathways are sensitive to the peptide structural flexibility. A relatively wide conformational space in the +1 charge state allows sufficient residue contact to facilitate radical migration, whereas narrower conformational space in the +2 charge state results in higher energy barriers to radical migrations. Folded

proteins are expected to have restricted conformational space due to high levels of intramolecular interactions, which should (in general) lead to larger kinetic barriers for migration. Results from this work suggest that radical migrations in proteins should be highly structure dependent, which should be beneficial for structure investigation.

Acknowledgments

The authors gratefully acknowledge funding from the National Science Foundation (CHE-074748).

References

- Dean, R.T., Fu, S.L., Stocker, R., Davies, M.J.: Biochemistry and pathology of radical-mediated protein oxidation. *Biochem. J.* **324**, 1–18 (1997)
- Hawkins, C.L., Davies, M.J.: Generation and propagation of radical reactions on proteins. *BBA Bioenergetics* **1504**, 196–219 (2001)
- Chu, I.K., Rodriguez, C.F., Lau, T.C., Hopkinson, A.C., Siu, K.W.M.: Molecular radical cations of oligopeptides. *J. Phys. Chem. B* **104**, 3393–3397 (2000)
- Headlam, H.A., Mortimer, A., Easton, C.J., Davies, M.J.: beta-scission of C-3 (beta-carbon) alkoxy radicals on peptides and proteins: A novel pathway which results in the formation of alpha-carbon radicals and the loss of amino acid side chains. *Chem. Res. Toxicol.* **13**, 1087–1095 (2000)
- Masterson, D.S., Yin, H.Y., Chacon, A., Hachey, D.L., Norris, J.L., Porter, N.A.: Lysine peroxy-carbamates: Free radical-promoted peptide cleavage. *J. Am. Chem. Soc.* **126**, 720–721 (2004)
- Hodyss, R., Cox, H.A., Beauchamp, J.L.: Bioconjugates for tunable peptide fragmentation: Free radical initiated peptide sequencing (FRIPS). *J. Am. Chem. Soc.* **127**, 12436–12437 (2005)

- Hao, G., Gross, S.S.: Electrospray tandem mass spectrometry analysis of *S*- and *N*-nitrosopeptides: Facile loss of NO and radical-induced fragmentation. *J. Am. Soc. Mass Spectrom.* **17**, 1725–1730 (2006)
- Lee, M., Kang, M., Moon, B., Oh, H.B.: Gas-phase peptide sequencing by TEMPO-mediated radical generation. *Analyst* **134**(8), 1706–1712 (2009)
- Ly, T., Julian, R.R.: Residue-specific radical-directed dissociation of whole proteins in the gas phase. *J. Am. Chem. Soc.* **130**, 351–358 (2008)
- Diedrich, J.K., Julian, R.R.: Site-specific radical directed dissociation of peptides at phosphorylated residues. *J. Am. Chem. Soc.* **130**, 12212–12213 (2008)
- Agarwal, A., Diedrich, J.K., Julian, R.R.: Direct elucidation of disulfide bond partners using ultraviolet photodissociation mass spectrometry. *Anal. Chem.* **83**(17), 6455–6458 (2011)
- Tao, Y., Quebbemann, N.R., Julian, R.R.: Discriminating D-amino acid-containing peptide epimers by radical-directed dissociation mass spectrometry. *Anal. Chem.* **84**(15), 6814–6820 (2012)
- Ly, T., Julian, R.R.: Elucidating the tertiary structure of protein ions in vacuo with site specific photoinitiated radical reactions. *J. Am. Chem. Soc.* **132**, 8602–8609 (2010)
- Zhang, X., Julian, R.R.: Investigating the gas phase structure of KIX with radical directed dissociation and molecular dynamics: Retention of the native structure. *Int. J. Mass Spectrom.* **308**, 225–231 (2011)
- Sun, Q.Y., Nelson, H., Ly, T., Stoltz, B.M., Julian, R.R.: Side chain chemistry mediates backbone fragmentation in hydrogen deficient peptide radicals. *J. Proteome Res.* **8**, 958–966 (2009)
- Chu, I.K., Zhao, J., Xu, M., Siu, S.O., Hopkinson, A.C., Siu, K.W.M.: Are the radical centers in peptide radical cations mobile? The generation, tautomerism, and dissociation of isomeric α -carbon-centered triglycine radical cations in the gas phase. *J. Am. Chem. Soc.* **130**, 7862–7872 (2008)
- Ng, D.C.M., Song, T., Siu, S.O., Siu, C.K., Laskin, J., Chut, I.K.: Formation, isomerization, and dissociation of α -carbon-centered and π -centered glycylglycyltryptophan radical cations. *J. Phys. Chem. B* **114**, 2270–2280 (2010)
- Wee, S., Mortimer, A., Moran, D., Wright, A., Barlow, C.K., O'Hair, R.A.J., Radom, L., Easton, C.J.: Gas-phase regiocontrolled generation of charged amino acid and peptide radicals. *Chem. Commun.* **40**, 4233–4235 (2006)
- Song, T., Ng, D.C.M., Quan, Q.A., Siu, C.K., Chu, I.K.: Arginine-facilitated α - and π -radical migrations in Glycylarginyltryptophan radical cations. *Chem Asian J* **6**, 888–898 (2011)
- Ly, T., Zhang, X., Sun, Q.Y., Moore, B., Tao, Y.Q., Julian, R.R.: Rapid, quantitative, and site-specific synthesis of biomolecular radicals from a simple photocaged precursor. *Chem. Commun.* **47**, 2835–2837 (2011)
- Dong, N.P., Liang, Y.Z., Yi, L.Z.: Investigation of scrambled ions in tandem mass spectra. Part I. Statistical characterization. *J. Am. Soc. Mass Spectrom.* **23**, 1209–1220 (2012)
- Moore, B.N., Julian, R.R.: Dissociation energies of X–H bonds in amino acids. *Phys. Chem. Chem. Phys.* **14**, 3148–3154 (2012)
- Blanksby, S.J., Ellison, G.B.: Bond dissociation energies of organic molecules. *Acc. Chem. Res.* **36**, 255–263 (2003)
- Jorgensen, W.L., Maxwell, D.S., TiradoRives, J.: Development and testing of the OPLS all-atom force field on conformational energetics and properties of organic liquids. *J. Am. Chem. Soc.* **118**, 11225–11236 (1996)
- Tsapraillis, G., Somogyi, A., Nikolaev, E.N., Wysocki, V.H.: Refining the model for selective cleavage at acidic residues in arginine-containing protonated peptides. *Int. J. Mass Spectrom.* **195**, 467–479 (2000)
- Wee, S., O'Hair, R.A.J., McFadyen, W.D.: Comparing the gas-phase fragmentation reactions of protonated and radical cations of the tripeptides GXR. *Int. J. Mass Spectrom.* **234**, 101–122 (2004)
- Ly, T., Julian, R.R.: Tracking radical migration in large hydrogen deficient peptides with covalent labels: Facile movement does not equal indiscriminate fragmentation. *J. Am. Soc. Mass Spectrom.* **20**, 1148–1158 (2009)
- Moran, D., Jacob, R., Wood, G.P.F., Coote, M.L., Davies, M.J., O'Hair, R.A.J., Easton, C.J., Radom, L.: Rearrangements in model peptide-type radicals via intramolecular hydrogen-atom transfer. *Helv. Chim. Acta* **89**, 2254–2272 (2006)